ADVANCED OPTICAL MATERIALS
www.advopticalmat.de

Label-Free Time-Resolved Monitoring of Photolipid Bilayer Isomerization by Plasmonic Sensing

*Jinhua Zhang, Francis Schuknecht, Ludwig Habermann, Alexander Pattis, Jonathan Heine, Stefanie D. Pritzl, Dirk Trauner, and Theobald Lohmüller**

The photo-isomerization of the photolipid *azo*-PC, a derivative of phosphatidylcholine containing an azobenzene group in its sn2 acyl chain, enables optical control over key properties of supported lipid bilayers (SLBs), such as membrane fluidity and bilayer thickness. However, azobenzenes are well-known for their interaction with various dyes through photo-modulation and -sensitization pathways, presenting a challenge in bilayer characterization by fluorescence microscopy. Label-free tools capable of monitoring the switching process of photolipid SLBs at the nanoscale are therefore highly desired. In this study, the use of dark field scattering spectroscopy on gold nanorods as a highly sensitive approach is demonstrated for analyzing the reversible photo-isomerization dynamics of photolipid SLBs in real time at the single particle level.

1. Introduction

Supported lipid bilayers (SLBs) are a versatile platform technology for emulating the lateral fluidity exhibited by native cell membranes on a solid support.[1] A remarkable feature of SLBs is their relative ease of formation, which has contributed to their widespread use in biophysical research. By drop-casting a solution of small unilamellar vesicles (SUVs) onto, for example, a clean glass substrate under buffered conditions, vesicle fusion, and extended bilayer formation can be achieved within minutes.[2] A thin water film separating the membrane and the substrate ensures that lipid mobility is sustained within the bilayer.[3]

Since the establishment of the SLB technology, various strategies have been reported for labeling SLBs with functional biomolecules, enabling the study of membrane organization,[4] membrane-protein interactions,[5] protein-protein interactions,[6] enzyme kinetics,[7] or cell-membrane interactions.[8] This progress has also inspired the development of new methods to control or restrict membrane organization and fluidity on SLBs, by applying electric fields[9] and temperature gradients,[10] physical barriers,[11] or nanoscale obstacles.[12] However, interfering with membrane properties in a reversible, fast, contactless, and localized fashion, compatible with physiological conditions, is not always straightforward. Light is ideally suited to meet all these demands, but this requires a photo-responsive bilayer membrane. In this regard, the use of photoswitchable lipids, or shortly photolipids, has emerged as a particularly useful strategy to obtain optical control over supported bilayer properties.

Azo-**PC**, a derivative of phosphatidylcholine containing an azobenzene group in its sn2 acyl chain, stands out as one of the most widely used photolipids.[13] When exposed to UV and blue light, the *azo*-**PC** lipids undergo reversible *cis/trans* isomerization. This photoisomerization process results in a fast change of bilayer thickness, density, and fluidity, providing a means to control membrane characteristics such as bending stiffness, domain formation, membrane permeability, and fusion.[13b,14] The efficiency of optical membrane control thereby depends on the photostationary state (PSS), which refers to the *trans/cis* photolipid ratio reached in a SLB under specific experimental conditions. For example, an *azo*-**PC** bilayer is only ≈4 nm thick, and the photo-isomerization from *trans* to *cis* can yield a membrane thinning of 5 and 10 Å in water and under buffered conditions, respectively.[15] This thickness change is further accompanied by an increase in the lipid cross-section.[14b] The difference observed in water and buffer solution can be attributed to a different PSS that is reached by the photolipid bilayer in each case. Analyzing such small changes on a single supported bilayer with sufficient spatio-temporal resolution is challenging and ex-

J. Zhang, F. Schuknecht, L. Habermann, A. Pattis, J. Heine, S. D. Pritzl, T. Lohmüller
Chair for Photonics and Optoelectronics
Nano-Institute Munich
Department of Physics
Ludwig-Maximilians-Universität (LMU)
Königinstraße 10, 80539 Munich, Germany
E-mail: t.lohmueller@lmu.de

S. D. Pritzl
Soft Condensed Matter and Biophysics Group, Department of Physics and Debye Institute for Nanomaterials Science
Utrecht University
Princetonplein 1, Utrecht 3584 CC, The Netherlands

D. Trauner
Department of Chemistry
College of Arts and Sciences
University of Pennsylvania
231 South 34th Street, Philadelphia, PA 19104-6323, USA

The ORCID identification number(s) for the author(s) of this article can be found under https://doi.org/10.1002/adom.202302266

DOI: 10.1002/adom.202302266

perimental methods that are suitable and sensitive enough are limited.

Arguably, the most widely applied methods for studying SLBs are fluorescence-based. The lateral distribution and diffusivity of fluorescent dyes within an SLB can be analyzed by Fluorescence Recovery After Photobleaching (FRAP), Fluorescence Correlation Spectroscopy (FCS), or Förster Resonance Energy Transfer (FRET), to name some of the most prominent examples.[16] However, one must consider that fluorophores can influence the photoisomerization dynamics of azobenzene through photosensitization and energy transfer,[17] which requires a careful selection of an appropriate fluorescent label. Standard lipid dyes can further affect the photoisomerization efficiency and the PSS reached in an *azo*-**PC** bilayer. Since the lipid photoswitch itself operates with light, label-free methods are therefore generally preferable.

Neutron[18] or X-ray scattering techniques, such as small angle X-ray scattering (SAXS),[14a,15] can accurately determine bilayer thickness of liposomes. However, capturing the switching dynamics with sufficient time resolution within a sub-µm spot-size can be challenging. In contrast, high-speed atomic force microscopy (AFM) offers both lateral and axial resolution in the nm range, making it suitable for observing lipid raft formation in SLBs of quaternary lipid mixtures containing photoswitchable ceramides.[19] With an AFM, the membrane is scanned from the top with a physical probe that is in contact with the bilayer. For measuring height differences, a reference point for the AFM tip is needed during imaging, such as a hole in the SLB or the presence of a membrane domain that remains at a constant height. Obtaining precise height differences can be challenging by AFM when a pure, defect-free *azo*-**PC** SLB, which can cover a surface area of a few cm^2, is homogeneously switched.

An alternative approach for label-free bilayer investigations is offered by plasmonic sensing. Plasmonic nanoparticles are well established as highly sensitive nanoscale probes for monitoring changes in the local refractive index of the embedding medium, via a measurable shift of the particle plasmon resonance. Additionally, they do not blink or bleach, which enables measurements over long timescales (up to hours and even days[20]). Plasmonic sensing has been successfully used to monitor protein binding[21] and protein-membrane interactions on supported bilayer membranes.[22] At the same time, the possibility of detecting azobenzene photoisomerization by plasmonic sensing has been demonstrated with gold nanoprisms functionalized with azobenzene containing, self-assembled monolayers (SAMs).[23] Inspired by these reports, we designed an experiment to investigate the isomerization dynamics of photolipids in an *azo*-**PC** SLB by plasmonic detection.

We utilized gold nanorods for the label-free monitoring of *azo*-**PC**-SLB photoswitching. The gold rods, stabilized by cetyltrimethylammonium bromide (CTAB) in solution, were first randomly deposited on the surface of a glass cover slip by drop-casting. Then, an SLB of *azo*-**PC** photolipids was formed via vesicle fusion of small liposomes. Lipid bilayer formation on top of the nanorods was observable with dark-field scattering microscopy by a red-shift of the nanorod's plasmon resonance peak. Furthermore, we show that continuous monitoring of the plasmon resonance peak for individual rods allows for monitoring time-resolved lipid photoisomerization and bilayer dynamics. Upon membrane photoisomerization with UV (λ = 365 nm) and blue (λ = 465 nm) light, a reversible plasmon resonance shift was observed due to the combination of a membrane thickness and membrane refractive index change. Both experimentally and by finite difference time domain (FDTD) calculations, we find that the magnitude of the observed plasmon peak shift is dependent on the nanorod coating and larger for plasma treated samples compared to CTAB stabilized particles. Overall, these results highlight the potential of plasmonic nanoparticles as sensitive probes for studying the dynamics of supported lipid bilayer membranes at the nanoscale with high accuracy.

2. Results and Discussion

Measurements were conducted with an upright darkfield microscope equipped with a spectrometer, as depicted in **Figure 1a**. Gold nanorods with an aspect ratio of 2.2 ± 0.1 nm (99.1 ± 3.4 nm × 44.2 ± 1.2 nm, CTAB coated) in water were dispersed on a glass cover slip by drop-casting to achieve random particle deposition on the substrate. The nanorods size distribution was analyzed by scanning transmission electron microscopy (STEM) (Figure S1, Supporting Information). The sample was rinsed multiple times with DI water to remove residual particles. Under the dark-field microscope, single nanorods are identifiable as red spots by their scattered light (Figure 1b). The particular gold nanorods were chosen for three main reasons. First, lipid membranes can coat nanoparticles with a diameter > 22 nm, as demonstrated for large unilamellar vesicles[24] and SLBs.[25] Second, gold nanorods are better suited for biosensing purposes compared to nanospheres, since they show weaker non-radiative damping and higher light scattering efficiencies.[26] Third, the nanorods exhibit a pronounced plasmon mode at ≈660 nm (Figure 1c), which is red-shifted from the wavelength range at which the photoswitch operates, and a small transverse plasmon mode at ≈530 nm (Figure S2, Supporting Information). To prevent membrane switching during dark-field spectroscopy, a 593 nm long-pass filter (LP593) was used to block light from the microscope lamp below this wavelength. This is crucial, since the broadband dark field illumination source could otherwise already be effective at switching photolipids in the gold nanoparticles' vicinity, via scattered light and high electromagnetic fields.

In the *trans* state, the absorption spectrum of *azo*-**PC** exhibits a maximum at ≈315 nm (Figure 1d,e). Undergoing photoisomerization with UV-A light, the *cis-azo*-**PC** absorption spectrum reveals a new band around ≈440 nm, corresponding to a S0 → S1 transition. Illumination with light in this wavelength range allows for back-switching of the photolipids to the *trans* state. Neither the *trans* nor the *cis-azo*-**PC** isomers display absorbance beyond 570 nm. Any photoisomerization attempt above this wavelength is therefore not effective. This was confirmed in control measurements with *azo*-**PC** liposomes that are irradiated with 630 nm light. Only minimal back-switching is observed in this case, even after prolonged illumination for 1 h (Figure S3, Supporting Information). Controlled photoisomerization was obtained by illuminating the SLB sample from the top with a UV (365 nm) and blue (465 nm) LED, which were both coupled through the objective (Figure 1b).

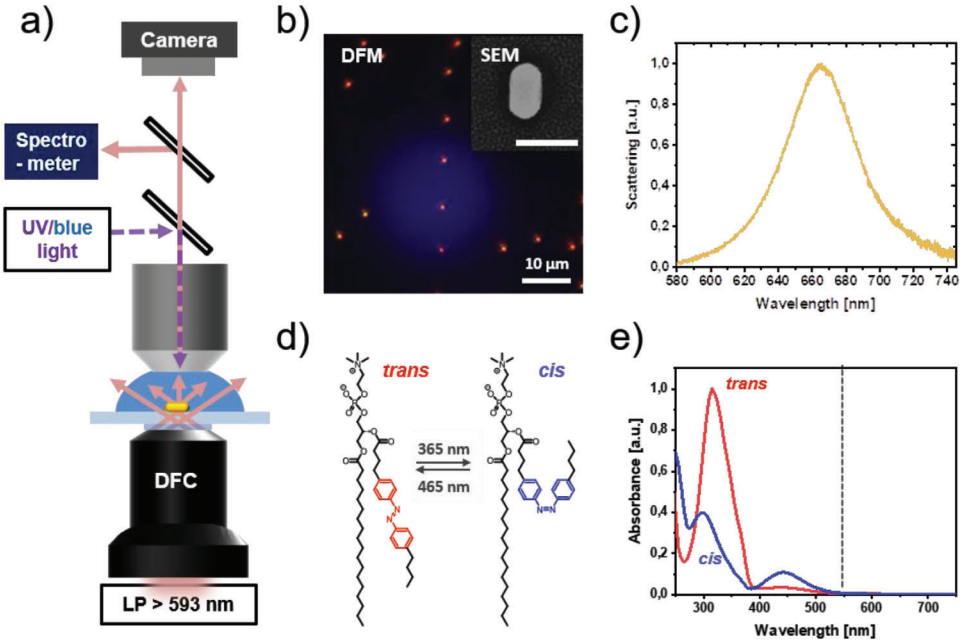

Figure 1. a) Experimental setup. Individual gold nanorods are detected in dark-field mode. UV and blue light are coupled through the objective to control membrane photoswitching. b) Dark field image of gold nanorods distributed on a glass cover slip. Individual particles are visible as red dots. The LED illumination spot with a diameter of ≈20 µm is visible in blue/purple. Inset: SEM image of a single gold nanorod (scale bar: 100 nm). c) Example scattering spectra of a single nanorod. d) Chemical structure of the photolipid *azo*-**PC**. Photoisomerization is obtained with UV-A and blue light illumination. e) Absorption spectra of *azo*-**PC** liposomes in the *cis* and *trans* state. Above 550 nm, both lipid conformations show negligible absorbance.

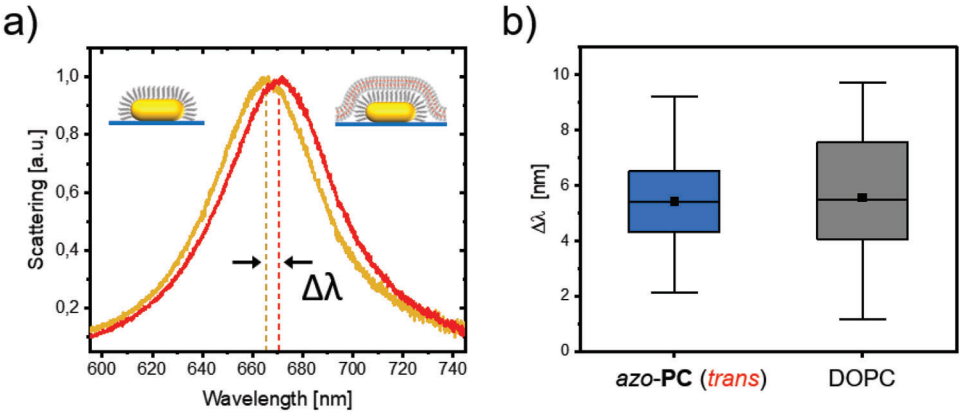

Figure 2. a) Scattering spectra are obtained from a single CTAB-coated gold nanorod before (golden line) and after (red line) sample coating with a dark-adapted, *trans-azo*-**PC** bilayer. A red-shift of the plasmon wavelength by $\Delta\lambda \approx 5$ nm is observed after SLB formation. b) Boxplot of the average plasmon peak shift ($\Delta\lambda_{trans\text{-}azo\text{-}\mathbf{PC}} = 5.49$ nm; N = 65 nanorods) after *trans-azo*-**PC** bilayer deposition. Control measurements with non-switchable DOPC (gray boxplot) show almost the same average plasmon shift $\Delta\lambda_{DOPC} = 5.55$ nm (N = 9 nanorods).

2.1. Plasmonic Sensing of SLB Formation and Photoswitching

Photolipid SLBs were formed on top of the gold rods by vesicle fusion of *azo*-**PC** SUVs. Prior to membrane formation, the SUVs were stored in darkness for over 24 h to ensure that the photolipids were converted to the thermodynamically preferred, dark-adapted *trans* state. Scattering spectra of individual gold nanorods were measured before and after the bilayer formation (**Figure** 2a). The shift of the plasmon resonance peak for each rod is analyzed by fitting its dark-field scattering spectrum with a Lorentzian function (Figure S4, Supporting Information). An average plasmon wavelength red-shift $\lambda_{azo-\mathbf{PC}} \approx 5.49$ nm is observed after adding the *azo*-**PC** vesicles (Figure 2b, blue box). This shift is indicative of a change in the nanorod's dielectric environment due to lipid bilayer covering the gold particles. We further performed control measurements with the non-switchable phospholipid DOPC (1,2-dioleoyl-sn-glycero-3-phosphocholine). For DOPC SLBs, an average red-shift of $\lambda_{DOPC} \approx 5.55$ nm was observed (Figure 2b, gray box). This shows that the refractive index change (Δn) due to membrane deposition is com-

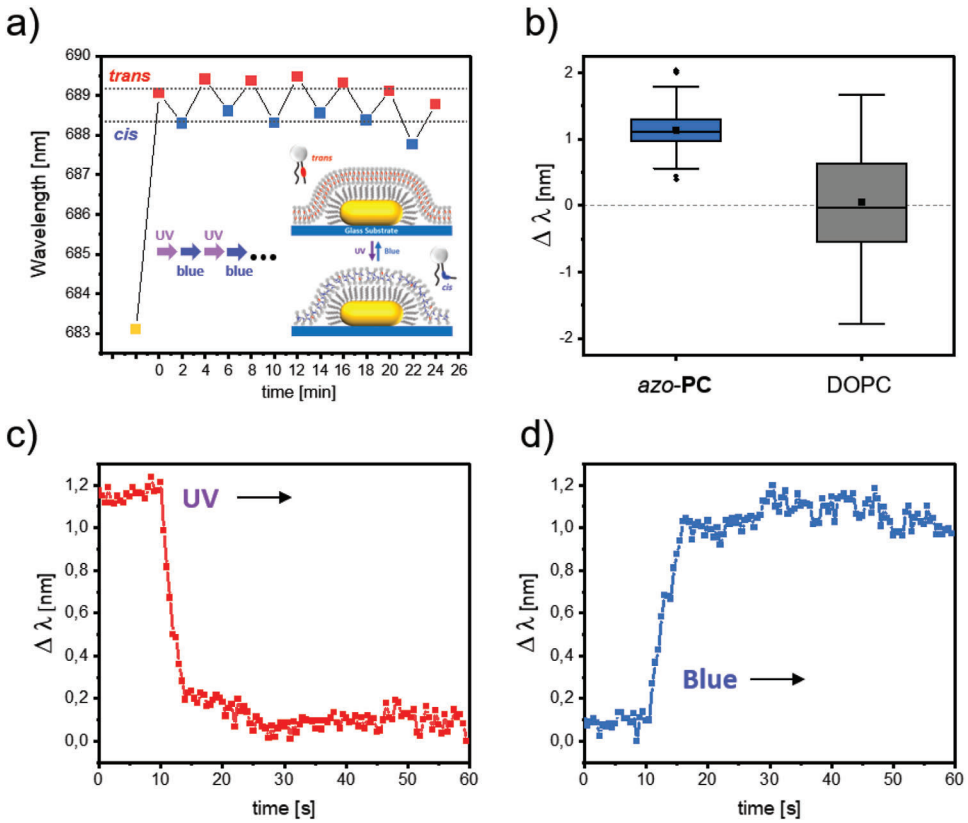

Figure 3. a) Reversible photoisomerization of an *azo*-**PC** bilayer measured by monitoring the peak shift of the nanorod's plasmon resonance. The plasmon resonance peak of the CTAB-coated nanorod prior to SLB formation is indicated by a yellow square. Sequential illumination with UV-A and blue light for 2 min respectively leads to reversible *cis* (blue squares)/ *trans* (red squares) membrane photoisomerization over many switching cycles. b) A median plasmon resonance shift $\Delta\lambda = 1.14$ nm was observed due to *azo*-**PC** photoisomerization (N = 15 nanorods; 58 switching cycles). Gray box: No peak shift was observed in control experiments with non-switchable DOPC ($\Delta\lambda = 0.04$ nm; N = 9 nanorods; 20 switching cycles). The observed plasmon resonance shift upon photoisomerization was significant with $p < 0.01$. c,d) Time-trace of the photoisomerization dynamics of the plasmon resonance shift for UV and blue illumination. Both LEDs were turned on at t = 10 s. A PSS was obtained within a few seconds for isomerization in *cis* and in *trans* direction.

parable in both cases. A DOPC and *trans-azo*-**PC** bilayer are of similar thickness. For DOPC, thickness values (d_{HH}: head-to-head) between 3.69[27] and 3.83 nm[28] have been reported. In comparison, the *azo*-**PC** bilayer thickness depends on the PSS, that is, its *trans/cis* ratio of lipids in the membrane. For the dark-adapted state (with ≈5% *cis*), a head-to-head-distance d_{HH} of 41.9 Å was reported, compared to a d_{HH} of 34.8 Å after UV light illumination.[14a] However, as mentioned earlier, these distances were also found to be solvent dependent. For example, in DI water, a maximum d_{HH} of only 39.0 Å was obtained after blue illumination, since a considerable fraction of lipids remained in the *cis* state. Based on these literature values, the value of bilayer thickness of DOPC can thus be assumed to lie between *trans* and *cis-azo*-**PC**. This is also the case for the area per molecule, which was reported to be 72.5 Å^2 for DOPC,[27] and between 78.6 and 56.6 Å^2 for *trans* and *cis-azo*-**PC**.[13a]

In the next step, the *azo*-**PC** SLB was subjected to an alternating illumination with UV and blue light through the objective (Figure 1a – the LED illumination spot is depicted in Figure 1b. Measured nanorods were aligned to be in the center of the illumination spot.). After a 2-min UV exposure to induce *trans*-to-*cis* membrane isomerization, a blue shift in the plasmon resonance peak was observed. This shift was entirely reversible by blue light illumination, which triggers *cis*-to-*trans* back-switching (**Figure 3a**)

Analyzing the data collected from 15 nanorods over 58 illumination cycles revealed an average shift of 1.14 nm for *azo*-**PC** due to isomerization (Figure 3b, blue box). Notably, this shift was exclusively observed in photolipid membranes. Control experiments with a non-photoswitchable DOPC SLB showed no considerable plasmon shift (Figure S5, Supporting Information). This also shows that the plasmon signal itself is not affected by the illumination sequence.

We further collected scattering spectra at a rate of 2 frames per second (fps) to determine the switching rates for the *azo*-**PC** SLB to reach its UV- or blue-adapted PSS. As depicted in Figure 3c,d, the photolipid bilayer reached a steady state within 10–20 s of illumination, as indicated by a constant signal in the time-trace. The switching rate for *trans*-to-*cis* was determined to be $k = 0.446$ s^{-1}, while back-switching exhibited at a rate of $k = 0.313$ s^{-1}. Notably, switching rates are not absolute but do depend on the illumination power density and wavelength of the individual light source.[29]

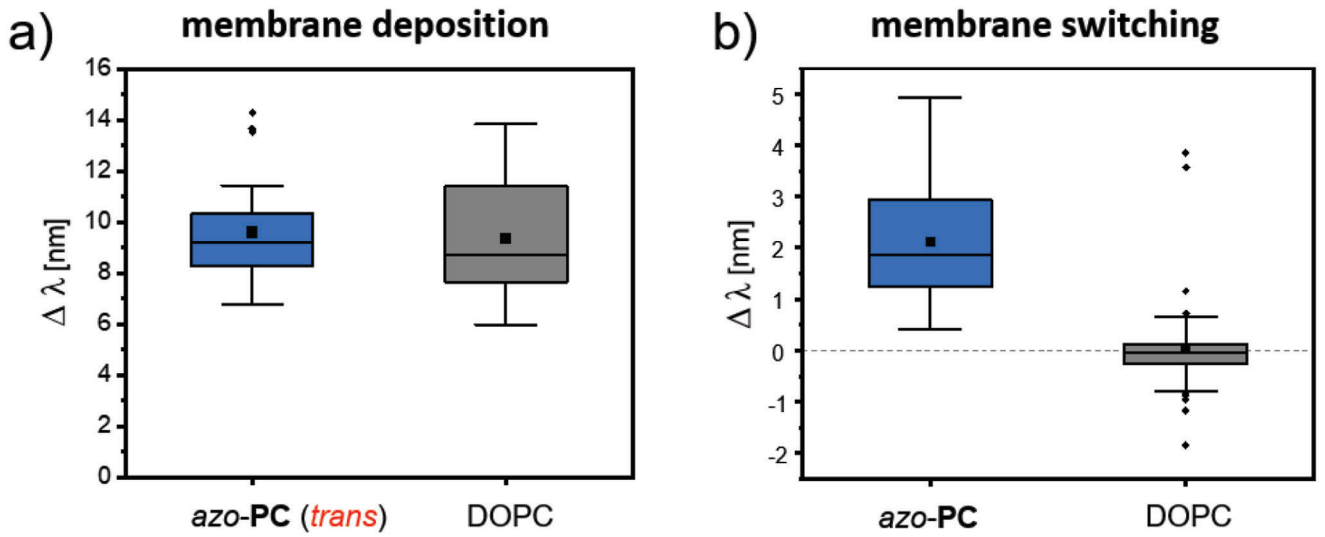

Figure 4. a) A plasmon resonance shift $\Delta\lambda = 9.59$ nm was observed after the deposition of *azo*-**PC** SLB (blue box) on a plasma treated nanorod sample (data obtained; N = 28 nanorods). For DOPC (gray box) a similar shift was observed after SLB deposition ($\Delta\lambda = 9.35$ nm, N = 12 nanorods). b) Plasmon resonance shift of plasma treated nanorods due to *azo*-**PC** photoswitching (blue box, $\Delta\lambda = 2.12$ nm, N = 8 nanorods; 49 switching cycles). Gray box: No peak shift was observed in control experiments with DOPC ($\Delta\lambda = 0.01$ nm; N = 15 nanorods; 33 switching cycles). The observed plasmon resonance shift upon photoisomerization was significant with $p < 0.01$.

2.2. Effect of Nanorod Coating

Having established the ability to monitor membrane isomerization through plasmonic sensing, we further aimed to characterize the impact of nanorod coating on the sensing performance. The measurements were thus repeated with nanorod samples that had undergone plasma cleaning to remove their CTAB coating (initially present to prevent aggregation of nanorods in solution).[30] Here, the average plasmon resonance shift after bilayer deposition was larger compared to the CTAB coated rods. An average shift of 9.59 nm was obtained for an *azo*-**PC** bilayer membrane and 9.35 nm for DOPC. (**Figure** 4a). The dark-adapted *trans-azo*-**PC** bilayer is ≈2–3 Å thicker than a DOPC bilayer, which agrees with the higher average red-shift of the plasmon wavelength observed after photolipid bilayer deposition. Note that for CTAB coated rods, no significant difference for the plasmon shift after SLB formation was observed between DOPC and photolipids, likely due to the overall lower sensitivity[30b] with increased nanorod-lipid distance, as explained in the following.

The plasmon resonance shift ($\Delta\lambda$) depends on the refractive index change of the surrounding dielectric medium (Δn) and the thickness of the adsorbate layer (d), which is expressed by[31]:

$$\Delta\lambda = m\Delta n\left(1 - e^{-2d/l_d}\right) \quad (1)$$

where l_d is the electromagnetic field decay length and m represents a sensitivity factor that is determined by the size, shape, and composition of the nanorods.[30b] The nanorods used in our experiment displayed an aspect ratio of 2.2 ± 0.1 nm, which is slightly more monodisperse than the aspect ratio of 2.2 ± 0.2 nm for nanorods of similar volume reported by Ye et al.[22d] For the latter, a refractive index sensitivity of ≈183 ± 5 nm per RIU was obtained, which means that refractive index changes of < 0.005 could be detected by the nanorod sensors. Furthermore, a sensing distance of ≈15 nm was estimated, which is almost three times higher than the thickness of a bilayer membrane. Based on these considerations, the nanorods should provide sufficient sensitivity to analyze *azo*-**PC** bilayer photoisomerization.

For a constant l_d, the larger average red-shift of the plasmon resonance peak observed for both DOPC and *azo*-**PC** SLB formation on the plasma cleaned sample can thus be explained by a closer proximity between the lipid bilayer and the nanorod surface. We also conducted reversible photoswitching experiments on plasma-treated nanorods, were an average plasmon wavelength shift of 2.12 nm was observed over multiple switching cycles (blue box in Figure 4b). Again, this larger peak-shift can be attributed to the exponential decay of the plasmons' electromagnetic field away from the nanorod's surface, yielding a higher sensitivity factor m in the absence of a CTAB layer. The conformation changes of the photolipids induced by photo-isomerization therefore result in a more pronounced signal. In this case, control measurements on DOPC membranes as shown in Figure 4b (gray box) were also performed.

As mentioned earlier, a thin water layer is formed between substrate and SLB, which keeps the bilayer fluid. For SiO_2 substrates, this water layer was reported to be in the range of 2–8 Å.[3] We have previously conducted FRAP measurements on *azo*-**PC** SLBs formed on glass and found that both blue and UV light illuminated membrane photolipids are mobile, although the diffusion coefficient D for a *trans* bilayer is by a factor of 2 lower compared to a *cis* bilayer (between D_{trans} ≈0.4 and D_{cis} ≈0.8 μm^2 s^{-1}).[14a] If only a local spot on a photolipid SLB is switched, both isomers can mix, which changes the *trans/cis* ratio and allows for an adjustment of the bilayer diffusivity.[14a] However, one must take under consideration that FRAP measurements only provide evidence for membrane fluidity over a large area on the whole substrate. This does not necessarily mean that the membrane itself is still fluid on top of the nanorods.

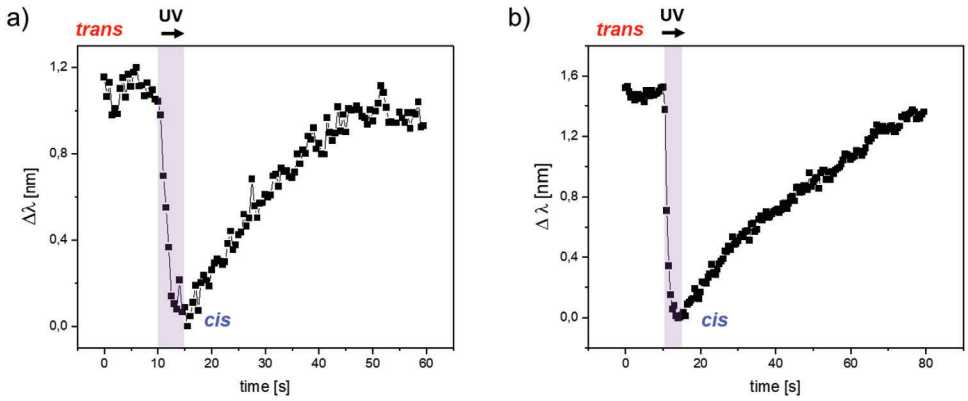

Figure 5. Probing SLB fluidity on a) CTAB coated and b) plasma treated nanorods. In both cases, a *trans-azo*-**PC** SLB was illuminated with 365 nm UV light for 5 s to switch the bilayer to a *cis*-rich state leading to a back-shift of the plasmon peak due to continuous dilution of the *cis-azo*-**PC** lipids with *trans* photolipids diffusing into the illumination spot.

For the CTAB stabilized or plasma cleaned gold nanorods, the formation of a water layer has not been reported, but one could assume a similar value for both DOPC and *azo*-**PC** due to their chemically identical head-groups. For CTAB coated particles, the formation of a fluid bilayer membrane has been demonstrated. Bare gold, however, has been characterized as a barrier material for lipid membranes, because lipids are more densely packed on gold, which could impair or even hinder bilayer fluidity.[11] For azobenzene SAMs it was also shown that reversible *trans/cis* photoisomerization requires a sufficient volume for each azobenzene-group to undergo a conformational change. Otherwise, steric hindrance between the molecules prevents the switching process. Notably, as shown in Figure 4b, photoisomerization is observed on plasma treated gold rods, which indicates that the azobenzene groups in the lipid tails have enough space to switch their conformation. The lipids are also not covalently attached to the substrate in a dense film, as it is the case for SAMs.

We conducted time-resolved measurements of the plasmon-shift to probe bilayer fluidity on single nanorods. Experiments were performed where individual particles covered by a *trans*-(blue adapted) *azo*-**PC** bilayer were illuminated with UV light through the objective. For these conditions, only photolipids within the illumination spot are switched to *cis*, while the majority of lipids of the extended SLB area (several mm^2) are unaffected. Each nanorod was illuminated for 5 s to reach the UV adapted, *cis*-rich PSS (**Figure 5**). For both the CTAB and plasma treated gold nanorods, a fast blue-shift of the plasmon resonance peak due to *trans*-to-*cis* isomerization was observed. After the UV light was turned off, the plasmon resonance shifted back to the initial value of the *trans*-SLB with a rate of ≈0.03 s^{-1} for $\Delta\lambda$ of the CTAB-nanorods and a slightly lower rate of ≈0.02 s^{-1} for the plasma treated sample. This back-shift is evidence for lipid mixing, that is, *cis*-photolipids diffusing out of the illumination spot, while *trans- azo*-**PC** lipids simultaneously diffusing into the spot. In other words, the *cis/trans* ratio of the SLB covering the nanorods is continuously decreasing. The *cis*-lipid fraction is diluted throughout the entire bilayer, and the plasmon resonance peak position indicative for a *trans*-rich SLB is recovered. Note, that this is, in principle, a similar concept as in FRAP, where fluorescence in a photobleached spot recovers over time, due to an exchange with non-photobleached lipids. FRAP thus allows to determine a membrane diffusion coefficient *D*. However, there is an important difference. The back-shift of the plasmon resonance peaks shown in Figure 5a,b is a result of lipid mixing and therefore a direct measure of the change of the local *trans/cis* ratio over time. Each time point corresponds to a different isomer ratio and accordingly to a different value of the local *D*.

2.3. Numerical Simulations

We conducted Finite Difference Time Domain (FDTD) simulations to gain a better understanding about the origin of the plasmon shift observed due to photoswitching (**Figure 6**). In particular, we compared the two scenarios of photolipid SLB formation on gold nanorods with and without CTAB coating. For the CTAB case, we used a model where the nanorod surface and the photolipid bilayer are separated by 3.6 nm, which corresponds to the average height of a CTAB coating reported in literature[32] (Figure 6a). For the plasma treated sample, we assumed that the photolipid bilayer is formed directly on the nanorod with no spacing in between (Figure 6b). The thickness of the dark-adapted *trans-azo*-**PC** bilayer was assumed to be 42 Å.[15] A water layer separating the bilayer from the substrate was not implemented in the calculation. Scattering spectra obtained from FDTD simulations are shown as Figure S6 (Supporting Information).

The plasmon shift for gold nanorods on a glass substrate that are covered by a 42 Å thick, *trans-azo*-**PC** bilayer is linearly dependent on the membrane refractive index, as shown with the red lines of Figure 6a,b. In the case of CTAB coated particles, the experimentally observed average plasmon shift $\Delta\lambda$ of 5.49 nm before and after bilayer deposition would correspond to a refractive index change from 1.33 (water) to 1.431 (*trans-azo-**PC***-SLB) (Figure 6a; red line). This is in good agreement with literature values for DOPC, where a refractive index between 1.435 and 1.450 has been reported.[33] Since the plasmon shift after *trans-azo-**PC*** and DOPC bilayer deposition was almost identical, a similar refractive index for both lipid membranes can be assumed. In comparison, the average plasmon shift of 9.59 nm for the plasma treated rods yields a refractive index shift from 1.33 (water) to 1.433. This shows that in both independent measurements the observed wavelength shifts after bilayer formation are consistent.

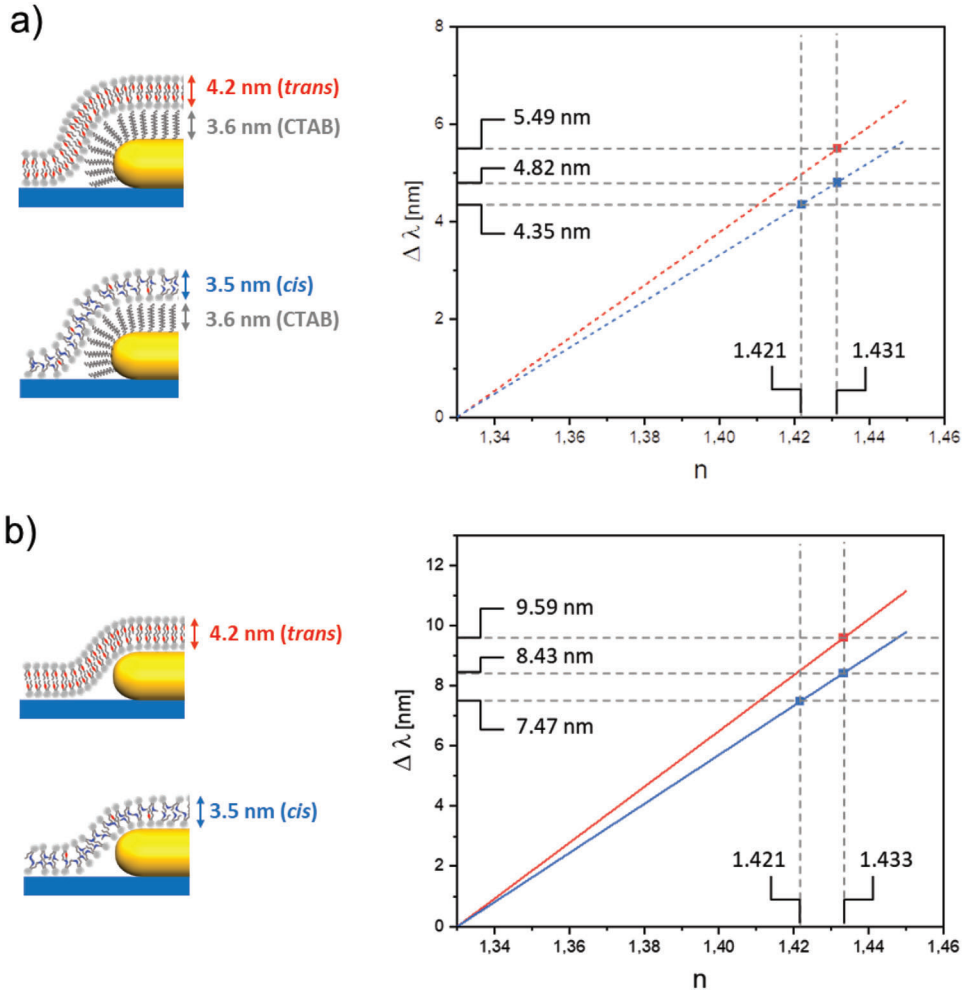

Figure 6. FDTD simulations of *azo*-**PC** SLB photoswitching. a) CTAB coated gold nanorods. b) Plasma treated sample. Red lines in both graphs represent the calculated dependence of the plasmon resonance shift on the refractive index of a 4.2 nm thick layer (corresponding to a *trans-azo*-**PC** SLB) coating of a gold nanorod on a glass substrate as illustrated in the sketches on the left. Blue lines represent the calculated dependence of the plasmon shift on refractive index for a 3.5 nm thick layer (corresponding to a *cis-azo*-**PC** SLB). The refractive index of water ($n = 1.33$) is the origin in all cases. The average plasmon shifts after bilayer deposition and membrane photoisomerization, as described in the main text, are highlighted by blue and red squares in the respective graphs. Dashed horizontal and vertical lines are guides to the eye.

To account for the reversible plasmon peak shift obtained by SLB photoisomerization, a change of *azo*-***PC*** bilayer thickness by 7 Å between *trans* and *cis* was assumed for the calculations. This value lies between the membrane thickness change of 5 Å reported for photolipid membranes in DI water and a change of 8–10 Å in buffered solution.[15]

A 7 Å thickness change yields a calculated blue-shift of the plasmon peak from 5.49 to 4.82 nm for CTAB-nanorods (Figure 6a; blue line) and from 9.59 to 8.43 nm for plasma treated particles (Figure 6b; blue line). This shows that the measured $\Delta\lambda$ of 1.14 and 2.12 nm, respectively, cannot be completely reproduced by only taking a thickness difference into account. However, by considering an additional refractive index change Δn of 0.01, the experimental results can be matched in both cases.

The small refractive index change can originate from a combination of effects. For example, the lipid density is different for a *trans* and *cis* bilayer, where *trans* lipids are more densely packed.[14b] Additionally, photoswitching of azobenzene will also result in a polarizability and thus a refractive index change. It was reported that the change of the refractive index between blue and UV light irradiated polyacrylates depends on the methylene $(\text{-CH}_2)_x$ spacer length. For 8 methylene groups, a Δn of ≈ 0.02 was determined, but it was also shown that the Δn was decreasing for increasing spacer length.[34] The refractive index change further depends on boundary conditions, such as the orientation of the azobenzene group. Based on these literature values a Δn of 0.01 obtained by membrane photoisomerization appears reasonable, although values obtained for polymer films cannot be directly translated to an *azo*-**PC** bilayer.

3. Conclusion

In conclusion, we have designed and characterized an approach to use gold nanorods as highly sensitive plasmonic probes for the time-resolved monitoring of the photoisomerization dynamics of *azo*-**PC** SLBs. The nanorod coating has an important influ-

ence on the probe sensitivity, where CTAB coated nanorods provide a smaller plasmon shift after bilayer deposition than plasma treated rods due to the higher spacing between the particle surface and the lipids. Time-resolved measurements of lipid mixing show that the bilayer fluidity on the nanorod surface is sustained in both cases. Furthermore, the nanorod sensing approach allows to study the photoisomerization dynamics of *azo*-**PC** not only after but also during blue and UV light illumination. A blue-shift of the plasmon resonance peak is observed upon switching the photolipid bilayer from a *trans*-rich to a *cis*-rich state. Through FDTD simulations, we have determined that this plasmon shift can be explained by a change in membrane thickness in the sub-nm range and a refractive index of the supported bilayers due to azobenzene isomerization. These findings open up opportunities for real-time monitoring of the photoswitching process and measurements of different photo-stationary states of *azo*-**PC** membranes using plasmon nanosensors. Plasmonic nanoantennas also provide large electromagnetic field enhancements upon resonant excitation with light, which can significantly enhance the Raman signal obtained from azobenzene close to the particle surface. Examples in literature have shown that the *cis/trans* ratio of azobenzene SAMs can be determined with high accuracy with such surface enhanced Raman spectroscopy (SERS).[35] The combination of plasmonic resonance sensing and SERS would not only provide insight into the membrane switching dynamics but could also be suitable for obtaining in situ information on the bilayer photostationary state during solvent exchange, temperature variation, or in response to other environmental influences. Furthermore, our results highlight the potential of plasmonic nanosensors not only for detecting molecular interactions and biological events occurring on membranes, but also for assessing changes in the membrane itself, such as conformational shifts and alterations in membrane composition and state.

4. Experimental Section

Sample Cleaning and Nanorod Deposition: Glass slides were cleaned with 50% ethanol (EtOH) and 50% Milli Q water twice, each for 30 min, and dried by air. Then, 100 µL deionized water was added onto the substrate, followed by adding 5 µL of the gold nanorod solution (Nanopartz Inc.,Part # A12-40-650). After allowing the gold rods to adsorb to the substrate for ≈ 1 min, remaining rods were removed by rinsing the sample with deionized water. Plasma cleaned nanorod samples were prepared in the same ways, except that after nanorod deposition the substrates were blown-dry with nitrogen and plasma cleaned for 75 s (air plasma, high power setting; Harrick).

Preparation of Photolipid SUVs and SLBs: The photolipid *azo*-**PC** was synthesized according to a previous protocol.[29] Small unilamellar vesicles (SUVs) samples of *azo*-**PC** or 1,2-Dioleoyl-sn-glycero-3-phosphocholine (DOPC; Sigma–Aldrich) were prepared by tip sonication. For this, 100 µL of lipids dissolved in chloroform at a concentration of 6.36 mM were pipetted in a dry round bottom flask. The chloroform was evaporated under a stream of air and nitrogen gas until a dry lipid film was obtained. The lipids were then rehydrated with 1.5 mL of deionized water and the sample was tip sonicated (BANDELIN electronic GmbH & Co. KG) twice, for 30 s on ice, until the solution was clear. Finally, the solution was centrifuged for 10 min at 8000 rpm and the supernatant containing SUVs was collected. To form an SLB on top of the gold nanorods, 100 µL of the SUVs solutions were diluted with 100 µL of PBS (1 ×) and pipetted onto the glass slide with pre-deposited gold nanorods. After 15 min, the SLB was formed and the remaining SUVs in solution were removed by rinsing the sample. Absorbance measurements were performed on *azo*-**PC** SUVs in DI water, using a Cary 60 UV–vis spectrophotometer.

Darkfield Scattering Spectroscopy/Microscopy: Scattering spectra from single gold nanorods were acquired using a dark field (DF) microscope (Zeiss Axio Scope A1) equipped with a DF oil immersion condenser (Zeiss 445323, 1.2–1.4). A 100 W halogen lamp (Zeiss) was used for DF illumination. A long pass filter (LP593) was used to prevent unwanted photoswitching of the photolipid membrane by cutting off blue and UV light from the lamp spectrum. Scattered light from single nanorods was collected with a 100 × water objective (NA = 1, Zeiss). A digital single-lens reflex camera (Canon EOS 6D) was used to acquire dark field images. Scattering spectra were measured with an Acton SP2500 spectrometer (Princeton Instruments). SLB photoswitching was realized using a UV- (365 nm, Prizmatix Mic-LED) and blue-LED (465 nm, Prizmatix Mic-LED), which were coupled through the objective. Measurements were conducted at constant temperature under ambient conditions. Control measurements were performed with a temperature sensor during illumination with the microscope lamp and the UV or blue LED, respectively (Figure S7, Supporting Information).

Supporting Information

Supporting Information is available from the Wiley Online Library or from the author.

Acknowledgements

This work was supported by the Deutsche Forschungsgemeinschaft (DFG) through the Collaborative Research Center SFB1032 (Project no. 201269156, Project A8). The authors thank local research clusters and centers such as the Center of Nanoscience (CeNS) for providing communicative networking structures. S.D.P. is supported by the Alexander-von-Humboldt foundation through a Feodor-Lynen fellowship. J.Z. is supported by the China Scholarship Council.

Open access funding enabled and organized by Projekt DEAL.

Conflict of Interest

The authors declare no conflict of interest.

Data Availability Statement

The data that support the findings of this study are available from the corresponding author upon reasonable request.

Keywords

azobenzene, photolipids, plasmonic sensing, supported bilayer membranes

Received: September 14, 2023
Revised: January 3, 2024
Published online: February 14, 2024

[1] a) J. T. Groves, S. G. Boxer, *Acc. Chem. Res.* **2002**, *35*, 149; b) E. Sackmann, *Science* **1996**, *271*, 43.
[2] E. T. Castellana, P. S. Cremer, *Surf. Sci. Rep.* **2006**, *61*, 429.
[3] B. W. König, S. Krueger, W. J. Orts, C. F. Majkrzak, N. F. Berk, J. V. Silverton, K. Gawrisch, *Langmuir* **1996**, *12*, 1343.

[4] H. P. Pace, J. K. Hannestad, A. Armonious, M. Adamo, B. Agnarsson, A. Gunnarsson, S. Micciulla, P. Sjövall, Y. Gerelli, F. Höök, *Anal. Chem.* **2018**, *90*, 13065.
[5] M.-P. Mingeot-Leclercq, M. Deleu, R. Brasseur, Y. F. Dufrêne, *Nat. Protoc.* **2008**, *3*, 1654.
[6] V. Kiessling, M. K. Domanska, D. Murray, C. Wan, L. K. Tamm, *Wiley Encycl. Chem. Biol.* **2008**, 1.
[7] H. Mao, T. Yang, P. S. Cremer, *Anal. Chem.* **2002**, *74*, 379.
[8] a) L. Kam, S. G. Boxer, *J. Biomed. Mater. Res.* **2001**, *55*, 487; b) R. Glazier, K. Salaita, *Biochim. Biophys. Acta, Biomembr.* **2017**, *1859*, 1465.
[9] M. Kandušer, M. Šentjurc, D. Miklavčič, *Eur. Biophys. J.* **2006**, *35*, 196.
[10] A. J. Walsh, J. C. Cantu, B. L. Ibey, H. T. Beier, Proc. SPIE 10062, Optical Interactions with Tissue and Cells XXCIII, **2017**.
[11] J. T. Groves, N. Ulman, P. S. Cremer, S. G. Boxer, *Langmuir* **1998**, *14*, 3347.
[12] T. Lohmüller, S. Triffo, G. P. O'Donoghue, Q. Xu, M. P. Coyle, J. T. Groves, *Nano Lett.* **2011**, *11*, 4912.
[13] a) S. S. Sandhu, Y. P. Yianni, C. G. Morgan, D. M. Taylor, B. Zaba, *Biochim. Biophys. Acta, Biomembr.* **1986**, *860*, 253; b) C. Pernpeintner, J. A. Frank, P. Urban, C. R. Roeske, S. D. Pritzl, D. Trauner, T. Lohmüller, *Langmuir* **2017**, *33*, 4083.
[14] a) P. Urban, S. D. Pritzl, M. F. Ober, C. F. Dirscherl, C. Pernpeintner, D. B. Konrad, J. A. Frank, D. Trauner, B. Nickel, T. Lohmueller, *Langmuir* **2020**, *36*, 2629; b) S. D. Pritzl, P. Urban, A. Prasselsperger, D. B. Konrad, J. A. Frank, D. Trauner, T. Lohmüller, *Langmuir* **2020**, *36*, 13509; c) P. Urban, S. D. Pritzl, D. B. Konrad, J. A. Frank, C. Pernpeintner, C. R. Roeske, D. Trauner, T. Lohmüller, *Langmuir* **2018**, *34*, 13368.
[15] M. F. Ober, A. Müller-Deku, A. Baptist, B. Ajanović, H. Amenitsch, O. Thorn-Seshold, B. Nickel, *Nanophotonics* **2022**, *11*, 2361.
[16] E. Sezgin, P. Schwille, *Cold Spring Harbor Perspective Biol.* **2011**, *3*, a009803.
[17] a) M. Shimomura, T. Kunitake, *J. Am. Chem. Soc.* **1987**, *109*, 5175; b) J. Ronayette, R. Arnaud, P. Lebourgeois, J. Lemaire, *Can. J. Biochem.* **1974**, *52*, 1848.
[18] J. Lemmich, K. Mortensen, J. H. Ipsen, T. Hønger, R. Bauer, O. G. Mouritsen, *Phys. Rev. E* **1996**, *53*, 5169.
[19] J. A. Frank, H. G. Franquelim, P. Schwille, D. Trauner, *J. Am. Chem. Soc.* **2016**, *138*, 12981.
[20] K. Kaefer, K. Krüger, F. Schlapp, H. Uzun, S. Celiksoy, B. Flietel, A. Heimann, T. Schroeder, O. Kempski, C. Sonnichsen, *Nano Lett.* **2021**, *21*, 3325.
[21] a) C. R. Yonzon, E. Jeoung, S. Zou, G. C. Schatz, M. Mrksich, R. P. Van Duyne, *J. Am. Chem. Soc.* **2004**, *126*, 12669; b) R. Ahijado-Guzmán, J. Prasad, C. Rosman, A. Henkel, L. Tome, D. Schneider, G. Rivas, C. Sönnichsen, *Nano Lett.* **2014**, *14*, 5528; c) G. Raschke, S. Kowarik, T. Franzl, C. Sönnichsen, T. A. Klar, J. Feldmann, A. Nichtl, K. Kürzinger, *Nano Lett.* **2003**, *3*, 935.
[22] a) C. Lambertz, A. Martos, A. Henkel, A. Neiser, T.-T. Kliesch, A. Janshoff, P. Schwille, C. Sönnichsen, *Nano Lett.* **2016**, *16*, 3540; b) C. L. Baciu, J. Becker, A. Janshoff, C. Sönnichsen, *Nano Lett.* **2008**, *8*, 1724; c) R. Ahijado-Guzman, J. Menten, J. Prasad, C. Lambertz, G. Rivas, C. Sönnichsen, *ACS Appl. Mater. Interfaces* **2017**, *9*, 218; d) W. Ye, S. Celiksoy, A. Jakab, A. Khmelinskaia, T. Heermann, A. Raso, S. V. Wegner, G. Rivas, P. Schwille, R. Ahijado-Guzman, *J. Am. Chem. Soc.* **2018**, *140*, 17901.
[23] a) S. D. Evans, S. R. Johnson, H. Ringsdorf, L. M. Williams, H. Wolf, *Langmuir* **1998**, *14*, 6436; b) G. K. Joshi, K. N. Blodgett, B. B. Muhoberac, M. A. Johnson, K. A. Smith, R. Sardar, *Nano Lett.* **2014**, *14*, 532.
[24] C. Contini, J. W. Hindley, T. J. Macdonald, J. D. Barritt, O. Ces, N. Quirke, *Commun. Chem.* **2020**, *3*, 130.
[25] Y. Roiter, M. Ornatska, A. R. Rammohan, J. Balakrishnan, D. R. Heine, S. Minko, *Nano Lett.* **2008**, *8*, 941.
[26] C. Sönnichsen, T. Franzl, T. Wilk, G. von Plessen, J. Feldmann, O. V. Wilson, P. Mulvaney, *Phys. Rev. Lett.* **2002**, *88*, 077402.
[27] J. F. Nagle, S. Tristram-Nagle, *Biochim. Biophys. Acta, Biomembr.* **2000**, *1469*, 159.
[28] P. Parkkila, M. Elderdfi, A. Bunker, T. Viitala, *Langmuir* **2018**, *34*, 8081.
[29] S. D. Pritzl, J. Morstein, S. Kahler, D. B. Konrad, D. Trauner, T. Lohmuller, *Langmuir* **2022**, *38*, 11941.
[30] a) G. W. Kim, J. W. Ha, *Phys. Chem. Chem. Phys.* **2020**, *22*, 11767; b) E. Martinsson, M. M. Shahjamali, N. Large, N. Zaraee, Y. Zhou, G. C. Schatz, C. A. Mirkin, D. Aili, *Small* **2016**, *12*, 330; c) M. Alba, N. Pazos-Perez, B. Vaz, P. Formentin, M. Tebbe, M. A. Correa-Duarte, P. Granero, J. Ferré-Borrull, R. Alvarez, J. Pallares, *Angew. Chem., Int. Ed.* **2013**, *52*, 6459.
[31] a) J. N. Anker, W. P. Hall, O. Lyandres, N. C. Shah, J. Zhao, R. P. Van Duyne, *Nanosci. Technol.* **2010**, *5*, 308; b) K. A. Willets, R. P. Van Duyne, *Annu. Rev. Phys. Chem.* **2007**, *58*, 267.
[32] M. J. A. Hore, X. Ye, J. Ford, Y. Gao, J. Fei, Q. Wu, S. J. Rowan, R. J. Composto, C. B. Murray, B. Hammouda, *Nano Lett.* **2015**, *15*, 5730.
[33] Z. Salamon, S. Devanathan, I. D. Alves, G. Tollin, *J. Biol. Chem.* **2005**, *280*, 11175.
[34] R. Yagi, H. Katae, Y. Kuwahara, S.-N. Kim, T. Ogata, S. Kurihara, *Polymer* **2014**, *55*, 1120.
[35] Y. B. Zheng, J. L. Payton, C.-H. Chung, R. Liu, S. Cheunkar, B. K. Pathem, Y. Yang, L. Jensen, P. S. Weiss, *Nano Lett.* **2011**, *11*, 3447.